Energy Reports 15 (2026) 109233

Contents lists available at ScienceDirect

Energy Reports

journal homepage: www.elsevier.com/locate/egyr

Research paper

Design principles and AC loss mitigation strategies for a 15 MVA HTS transformer

Asef Ghabeli [a,*], Mathias Noe [a], Stephan Rother [b], Christian Schacherer [b], Aime Mbuy [b], Jürgen Gangel [c], Francesco Grilli [a]

[a] Institute for Technical Physics, Karlsruhe Institute of Technology, Karlsruhe, Germany
[b] Siemens Energy, Erlangen, Germany
[c] Siemens Energy, Weiz, Austria

ARTICLE INFO

Keywords:
HTS transformer
AC loss
Finite element method
Roebel cable
Design criteria
Wind generator transformer

ABSTRACT

Offshore wind generators are expected to exceed 15 MVA in the coming years, necessitating compact and light-weight step-up transformers. While high-temperature superconducting (HTS) transformers offer high efficiency and compact size, their complex AC loss behavior in large-scale devices is still not sufficiently understood. In this work, we present a comprehensive investigation on practical strategies for reducing AC loss in a 15 MVA HTS transformer based on the primary industrial criteria of efficiency, weight, and cost. We employed an efficient numerical method to model up to thousands of HTS tapes in low-voltage (LV) and high-voltage (HV) windings in detail. Using this framework, we evaluated the influence of key design and operating parameters on the AC loss, including winding height, axial gap between the cables, radial distance between HV and LV windings, winding height difference, number of parallel conductors, voltage per turn, magnetic flux diverters, and temperature. These analyses enable the development of four improved transformer designs at operating temperatures of 20 K, 70 K, and two configurations at 77 K that balance AC loss reduction with conductor cost and core weight. The results provide validated design principles and practical guidelines for developing next-generation HTS transformers that are compact, light-weight, cost-effective, and suitable for large-scale offshore wind energy systems.

1. Introduction

Offshore wind power systems are expected to experience significant growth in the coming years (U.S. Department of Energy, 2023). Simultaneously, the capacity of wind generators to connect the generator voltage level to the grid voltage level is anticipated to surpass 15 MVA, necessitating the use of transformers to match this increased capacity. Due to the very low generator voltage level, wind generator transformers require a high voltage ratio and a very high current on the low-voltage side (Jose and Chacko, 2014). Meeting these demands while maintaining a lightweight and compact design is essential for minimizing nacelle mass, thereby reducing both installation and maintenance costs in large-scale offshore wind farms.

Since high-temperature superconductors (HTS) offer a very high current density, they are a promising solution for future compact and lightweight transformers with minimal AC losses. Their unique electromagnetic properties allow for substantial reductions in transformer volume and weight, improve the energy efficiency and lower the operational costs for offshore renewable energy systems. Consequently, HTS transformers are recognized as a promising solution for future high-capacity offshore wind applications.

Since the development of the first HTS transformer in 1996 (Zueger, 1998), numerous HTS transformers have been constructed and tested globally (Schlosser et al., 2003; Glasson et al., 2013; Dai et al., 2016; Glasson et al., 2017). At KIT, an HTS transformer with active fault current limitation using HTS tapes was designed (Berger, 2011; Berger et al., 2011) and a 1 MVA HTS transformer (HTS only on low-voltage side) was fabricated and tested in cooperation with ABB (Hellmann et al., 2017, 2019). A 1 MVA HTS transformer was constructed and tested in New Zealand using HTS Roebel cable for the first time (Glasson et al., 2013, 2017). In 2023, a 6.6 MVA HTS traction transformer was fabricated and tested with efficiency above 99%.

The AC loss in an HTS transformer winding originates from transport current and magnetization current; the latter is also known as shielding or screening current (Kajikawa and Funaki, 2012). The magnetization current is induced by the leakage magnetic field. In windings made of second-generation (2G) HTS tapes, it is mainly caused by

* Corresponding author.
E-mail address: asef.ghabeli@kit.edu (A. Ghabeli).

https://doi.org/10.1016/j.egyr.2026.109233
Received 15 December 2025; Received in revised form 24 February 2026; Accepted 8 March 2026
Available online 17 March 2026

the magnetic field component perpendicular to the wide face of the tape. The magnetization current is undesirable because it contributes to additional AC loss and diminishes the tape capacity to carry transport current. Additionally, the perpendicular magnetic field component decreases the critical current of the tape, further reducing its capacity to carry the transport current.

The primary challenge in designing an HTS transformer with reduced AC loss is the implementation of strategies to effectively minimize the perpendicular component of the leakage magnetic field. The leakage magnetic field is highly sensitive to geometric variations in the magnetic components of the transformer. Therefore, the detailed modeling of the windings and other magnetic components becomes essential for accurately calculating and mitigating AC loss in HTS transformers.

Numerical modeling serves as an efficient tool for estimating AC loss and facilitating the optimized design of HTS transformer. (Ghabeli et al., 2015b; Ghabeli and Besmi, 2017; Kim et al., 2005b; Li et al., 2008; Ghabeli et al., 2015a; Song et al., 2018, 2020; Fang et al., 2021; Jiang et al., 2021; Wu et al., 2023). For systems with thousands of 2G HTS tapes exhibiting a high width-to-thickness ratio, employing a fast and efficient model such as the 2D axis-symmetric T-A formulation is essential. The T-A formulation in 2D was introduced in 2017 to address the challenge of modeling 2G superconducting coils or stacks with a very large number of turns (Liang et al., 2017). Studies have shown that 2D axis-symmetric T-A models have a good agreement with 2D axis-symmetric H-formulation models, 3D T-A models, and experiments when modeling coils and windings (Wu et al., 2023; Vargas-Llanos et al., 2021, 2020, 2023, 2022; Li et al., 2021).

In this paper, we present a comprehensive study on practical strategies for reducing AC loss in a 15 MVA HTS transformer based on the three main industrial criteria of efficiency, weight, and cost. We introduce the design criteria and the modeling strategy in Section 2, while the HTS transformer specifications and winding configurations are described in Section 3. The subsequent sections analyze the effect of several design parameters on AC loss: the winding height and axial gap between cables (Section 4); the radial spacing between the LV and HV windings and their height difference (Section 5); the number of parallel conductors (Section 6); the voltage per turn (Section 7); and the inclusion of an iron core and magnetic flux diverters (Section 8). Finally, Section 9 discusses the effect of operating temperature on AC loss and proposes four improved transformer designs at 20–77 K.

2. Methodology

2.1. Design criteria

Although the primary objective of this work is to develop an improved HTS transformer design for AC loss mitigation, three main design criteria were considered: efficiency, weight and cost. Focusing on only one of these criteria would not lead to a realistic design. For instance, the AC loss can be significantly reduced by using multiple HTS tapes in parallel; however, this simultaneously increases the conductor length, and hence the overall cost.

2.1.1. Cost

The most significant contributors to the total cost of an HTS transformer are the cooling system and the HTS conductor. In this study, we simplified the cost evaluation by considering only the length of the HTS material, which is directly proportional to its cost. The cost of the cooling system depends on multiple factors such as design of the cryostat, cooling power and operating temperature, which requires a dedicated study beyond the scope of this work.

2.1.2. Weight

The total weight of an HTS transformer consists of several components, including cryostat, superconducting windings, mechanical framework, current leads, cooling system, and liquid nitrogen (LN_2). To simplify the comparison between different designs, only the magnetic core weight was included in the evaluation. This approximation is reasonable since the core typically accounts for roughly 40%–60% of the total transformer weight (Kalsi, 2011; Zhao et al., 2023).

2.1.3. Efficiency

We evaluated the transformer efficiency based only on the AC loss in the HTS windings, while other loss components were neglected. In an HTS transformer, additional loss is generated by eddy current loss in iron core, ohmic loss in current leads and cryostat loss. The importance of each contribution to the total loss varies based on the operating temperature and the load value, but their accurate calculation requires a detailed study, which is out of the scope of this paper. Since the AC loss in the HTS windings generates the dominant variable loss at full loads, this simplifications provides a reasonable basis for comparing different design configurations.

In this context, the specific parameter ranges investigated in this study (e.g. axial gap between cables, windings height, radial distance between windings, number of the strands in the Roebel cable, voltage per turn and operating temperature) were selected to reflect realistic industrial designs. These ranges follow design norms that are used in conventional and HTS transformer engineering. Such norms are based on extensive experience that are obtained from previously designed and tested transformers in order to balance electromagnetic performance, mechanical feasibility, dielectric requirements, and economic considerations. Therefore, the selected ranges ensure that the parametric study investigates configurations that are both technically meaningful and directly relevant to practical transformer design.

2.2. Modeling strategy

With the T-A formulation model, the thin superconducting layer in a 2G HTS tape is modeled as a 1D element. This approach has two advantages: firstly, it eliminates the **T** variable parallel to the tape's width, and secondly, it resolves the problematic mesh with a very high width-to-thickness ratio in the 2G HTS tape. Since the fundamentals of the T-A formulation are widely discussed in the literature, we refer the readers to previous articles (Zhang et al., 2017a; Zhou et al., 2022; Huber et al., 2022; Zhou et al., 2023).

For modeling the non-linear characteristics of the superconducting material, we use an $E-J$ power law as

$$\mathbf{E}(\mathbf{J}) = E_c \left(\frac{|\mathbf{J}|}{J_c(\mathbf{B})} \right)^n \frac{\mathbf{J}}{|\mathbf{J}|}, \tag{1}$$

where $E_c = 10^{-4}\ \mathrm{V\,m^{-1}}$ is the critical electric field, $J_c(\mathbf{B})$ is the critical current density dependent on the amplitude and orientation of the magnetic field, and n is the power exponent that identifies the steepness of the current–voltage curve. We use an extended version of the conventional Kim's model to describe the field-dependent critical current density (Kim et al., 1962; Zhang et al., 2017b):

$$I_c(B,\theta) = I_{c0} \cdot \left(1 + \sqrt{\frac{\sin^2(\theta)}{\gamma} + \cos^2(\theta)} \cdot \left(\frac{B}{B_0} \right)^{\alpha} \right)^{-\beta}, \tag{2}$$

where I_{c0} is the self-field critical current, B is the magnitude of magnetic flux density and B_0 and β are empirical parameters. The parameter γ accounts for the angular anisotropy of the HTS tape and α is an empirical factor introduced in Zhang et al. (2017b) to achieve a better fit with the experimental data.

The time-averaged AC loss over a cycle (in watts) in the 2D axis-symmetric T-A model is obtained as:

Table 1
Main parameters of the studied 15 MVA wind turbine transformer.

Parameter	Value
Rated power	15 MVA
Nominal voltage (HV, LV)	66 kV, 690 V
Maximum voltage (HV, LV)	72.5 kV, 1 kV
Rated current (HV, LV)	131 A, 12.55 kA
Short-circuit impedance	17%
Frequency	50 Hz
Core maximum field density	1.2 T

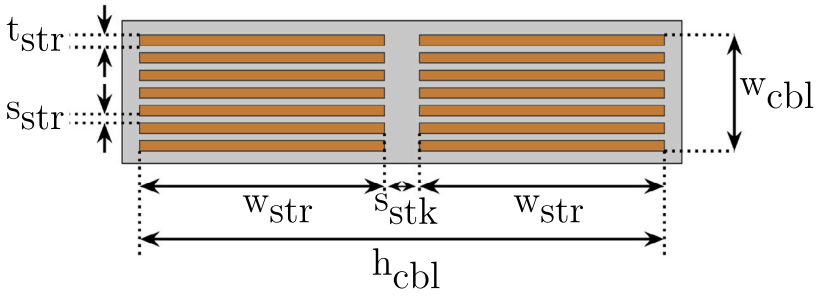

Fig. 1. Schematic of the cross-section of a Roebel cable with its parameters. The cable is rotated by 90° compared to its geometry in the model.

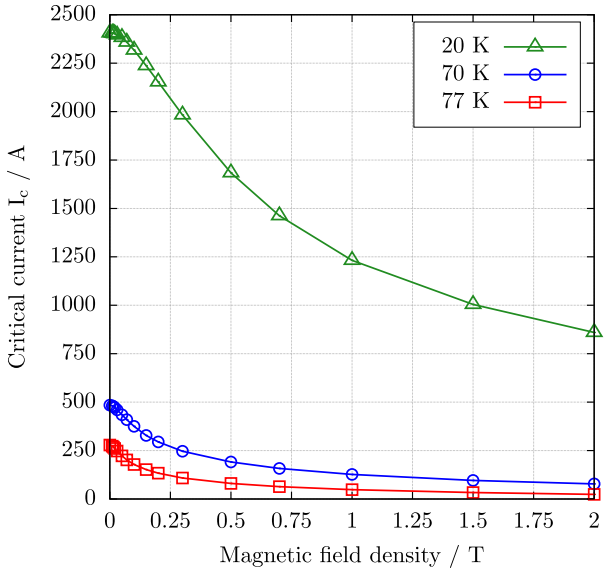

Fig. 2. Measured critical current of 4 mm Fujikura FYSC tape at 20 K, 70 K and 77 K under perpendicular external magnetic field up to 2 T. The data were provided by Robinson Research Institute in New Zealand from measurements performed at their SuperCurrent facility (Strickland et al., 2014).

$$P = 2\pi r \cdot \frac{2}{T} \int_{T/2}^{T} \left(\iint_{\Omega_{sc}} \mathbf{E} \cdot \mathbf{J} \, ds \right) dt, \tag{3}$$

where Ω_{sc} is the superconducting domain.

2.3. Modeling limitations and assumptions

In the present model, we assume the critical current density to be uniform along both the length and width of the HTS tapes, although this does not fully reflect real-world conditions (Gömöry et al., 2019; Solovyov et al., 2013). This assumption, particularly the neglect of lateral non-uniformity of critical current density may lead to an underestimation of the absolute AC loss values; however, the general trend and relative comparisons of AC loss are expected to remain unchanged.

Furthermore, the model does not include the metallic layers of the HTS tape and therefore neglects eddy current losses in those layers (Pardo et al., 2015). The contribution of eddy current losses strongly depends on frequency and operating temperature. At grid-relevant frequencies and operating temperatures above approximately 50 K, eddy current losses can be neglected compared to the hysteresis loss in the superconducting layer. However, at cryogenic temperatures below about 50 K, eddy current losses in the metallic layers are no longer negligible due to the significant reduction in electric resistivity, which leads to higher eddy currents (Mellerud et al., 2024). Therefore, at the lowest investigated temperature in this study (20 K), neglecting metallic eddy current losses may lead to an underestimation of the absolute value of AC loss. Nevertheless, the qualitative extracted trends are expected to remain valid.

3. Transformer specification and winding configuration

3.1. Transformer specification

Table 1 summarizes the main parameters of the studied 15 MVA HTS transformer. The transformer connects the 66 kV grid to the 690 V generator voltage level. In a separate study, we demonstrated through calculations that in a shell-type core three-phase transformer, the total AC loss in HV and LV windings differs by only about 5% between the middle and outer limbs. That is why here we focus only on one phase out of three phases, assuming similar AC loss across all phases. We chose a concentric arrangement for both HV and LV windings due to its significantly lower AC loss compared to the reciprocal arrangement (K. et al., 2005a).

3.2. Low-voltage winding

For the design of the LV winding, we selected a Roebel cable composed of 14 strands. The Roebel cable is one of the few practical fully transposed HTS superconducting cables (Glasson et al., 2013, 2017). Transposition of tapes in a cable is necessary to reduce the circulating current and AC loss. The schematic layout and geometric parameters of the cable's cross section are illustrated in Fig. 1. The Roebel cable was designed using Fujikura FYSC 2G HTS tape. Table 2 summarizes the cable and tape specifications.

Fig. 2 shows the reduction of critical current under external magnetic fields of up to 2 T for 4 mm Fujikura tape obtained from the

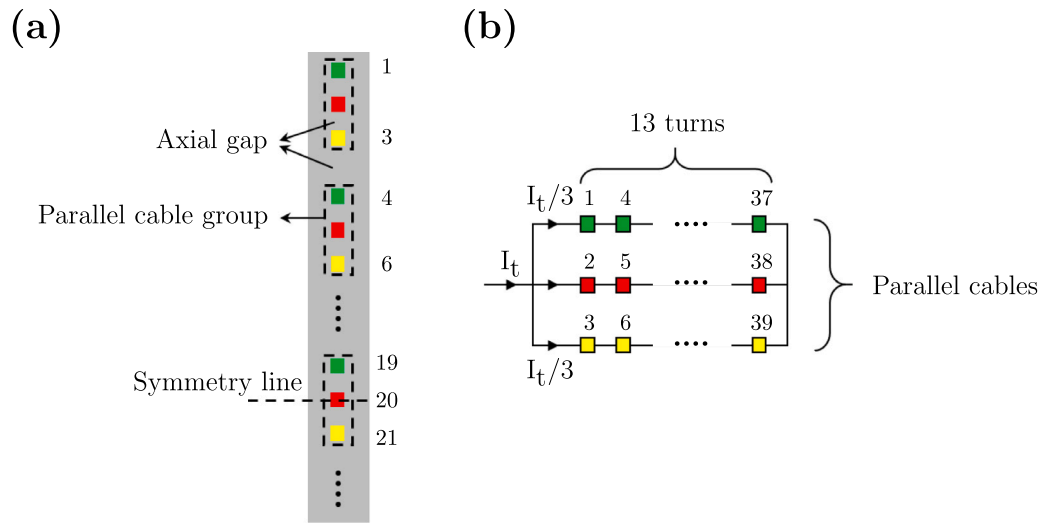

Fig. 3. LV Winding of the designed HTS transformer at 20 K and winding voltage of 45 V: (a) Configuration schematic; (b) Circuit diagram.

Table 2
Geometric parameters of the selected Roebel cable and Fujikura FYSC tape used in the cable (see schematic in Fig. 1).

Parameter	Symbol	Value
Roebel Cable		
Number of strands/–	n_{str}	14
Strand width/mm	w_{str}	4.0
Strand thickness/μm	t_{str}	2.0
Strand separation/mm	s_{str}	0.108
Inter-stack separation/mm	s_{stk}	1.0
Total cable height/mm	h_{cbl}	9.0
Total cable width/mm	w_{cbl}	0.77
Fujikura FYSC 2G HTS Tape		
Tape width/mm	–	4.0
Total tape thickness/mm	–	0.11
Superconducting layer thickness/μm	–	2.0
Substrate thickness/μm	–	50
Copper stabilizer thickness/μm	–	20

Table 3
Geometric parameters of the HV and LV windings at 20 K and winding voltage of 45 V.

Parameter	LV	HV
Radius/mm	334.5	380.5
Height/mm	661	658
Parallel conductor[a] (Axial, Radial)/–	3, 1	1, 1
Axial turns per full layer/–	39	110
Axial turns in last layer/–	N/A[b]	51
Radial layers (full + partial)	1	8 + 1
Total turns/–	13	931
Axial gap/mm	8	2
Radial gap/mm	N/A	2
Conductor length/km phase^{-1}	1.115	2.225
Core weight/t[c]	9.682	

[a] We use "conductor" everywhere in the paper to refer to cables or tapes.
[b] LV has no partial last layer; last layer equals a full layer.
[c] t stands for tonne.

Wimbush database and measured at the SuperCurrent facility at Robinson Research Institute (Strickland et al., 2014). The self-field critical currents of the 4 mm tape at 20 K, 70 K and 77 K are 2405 A, 485 A and 279 A, respectively.

Table 3 shows the geometric parameters of the selected LV winding adopted for the design at 20 K, and Fig. 3 shows the LV winding schematic. Throughout this paper, the operating temperature is assumed to be 20 K, unless stated otherwise. Only in Section 9 (Influence of operating temperature), we investigate the design at different temperatures (20 K, 70 K, and 77 K).

At a winding voltage of 45 V, the LV winding consists of 13 turns, each composed of three parallel Roebel cables. Consequently, each cable carries one-third of the nominal current. Since the strands within each cable are fully transposed, an equal current distribution among the strands is considered a realistic assumption. The axial gap between the parallel cables within a cable group is always considered to be equal to the gap between adjacent parallel cable groups. Owing to the symmetry of the winding, only the top half of the winding is modeled in all the simulations.

3.3. High-voltage winding

Table 3 shows the geometric parameters of the HV winding configuration at 20 K. At a winding voltage of 45 V, the HV winding is comprised of 931 turns of 4 mm Fujikura tape. The Fujikura tape used

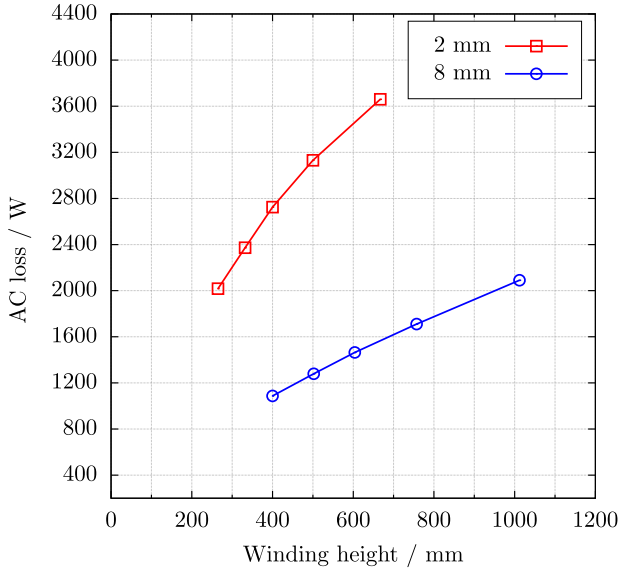

Fig. 4. Effect of winding height on the AC loss in the single LV winding configuration. The height were increased by increasing the number of turns. All the cases were calculated under full-load condition.

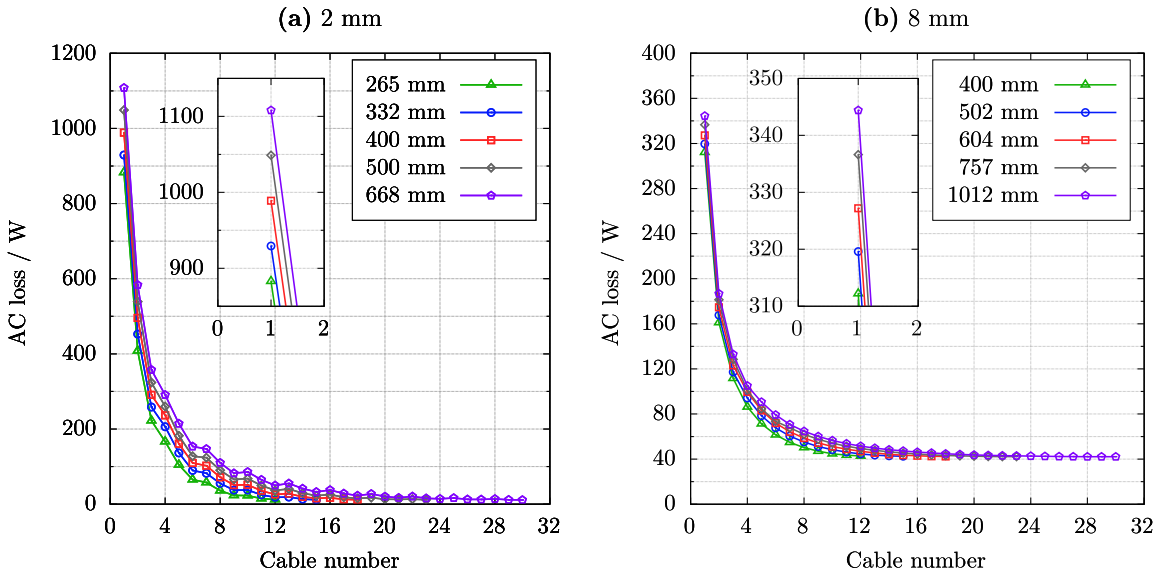

Fig. 5. Comparison of the AC loss distribution among cables in the single LV winding configuration for different winding heights: (a) 2 mm axial gap, (b) 8 mm axial gap. The height were increased by increasing the number of turns. All the cases were calculated under full-load condition. The zoomed inset plots are highlighting the end cables with the highest AC loss values.

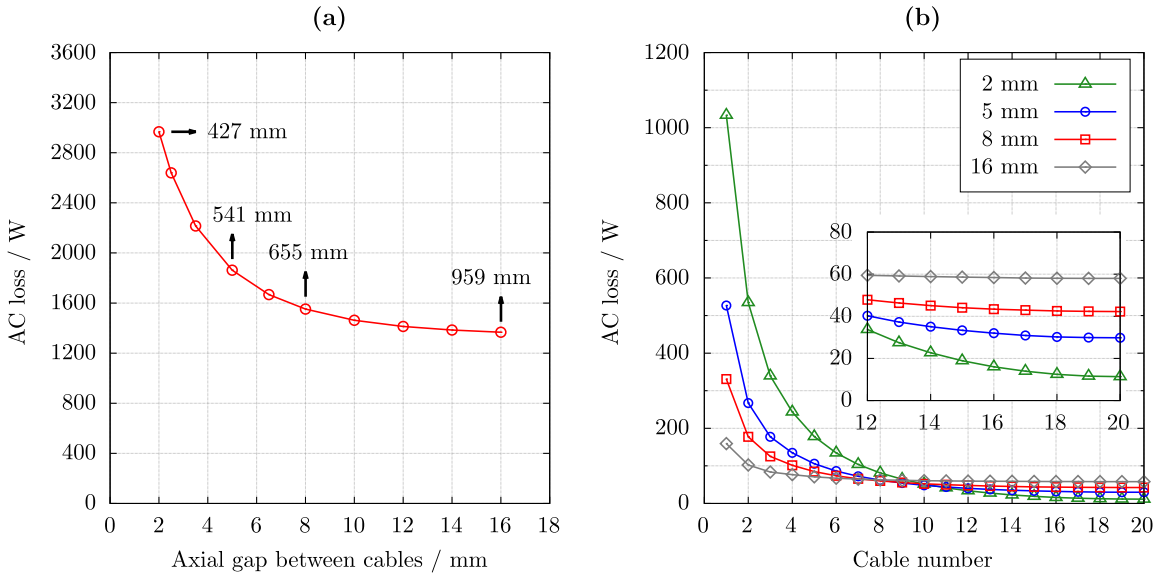

Fig. 6. (a) Effect of axial gap between cables on the AC loss of LV winding in the single LV winding configuration. (b) AC loss distribution among cables for different axial gap values. All cases were calculated under full-load condition.

in the HV winding has the same characteristics as the tape described in Table 2.

4. Influence of winding height and axial gap

4.1. Single low-voltage winding

Increasing the axial gap between the cables within a winding results in an increase of its overall height. To decouple these two effects, we first analyze the impact of increasing the winding height independently, by increasing the number of turns while keeping the axial gap constant. Afterwards, the effect of increasing the axial gap can be investigated more realistically.

In this study, we classify the axial gap into two types: a small axial gap represented by a 2 mm gap and a large axial gap represented by a 8 mm gap. Although we investigate various axial gaps in detail in this section, we focus only on 2 mm and 8 mm gaps in the following sections for sake of conciseness.

The winding height was increased by varying the number of turns for two different axial gaps: 2 mm and 8 mm. The number of turns was set equal to 8, 10, 12, 15 and 20, resulting in winding heights ranging from 265 mm to 668 mm for 2 mm axial gap, and from 400 mm to 1012 mm for 8 mm axial gap.

Fig. 4 shows that the AC loss increases with winding height when the axial gap between the cables is kept constant. The increase is approximately 2.5 times higher in the windings with 2 mm axial gap compared to 8 mm axial gap. This trend can be explained by the AC loss distribution shown in Fig. 5(a) and (b). The majority of the AC loss occurs in the end cables, where the loss for the 2 mm axial gap is roughly 3 times higher than for the 8 mm gap. In contrast, the middle cables show higher AC losses in the windings with an 8 mm axial gap (approximately 40 W) than in those with a 2 mm gap (around 10 W).

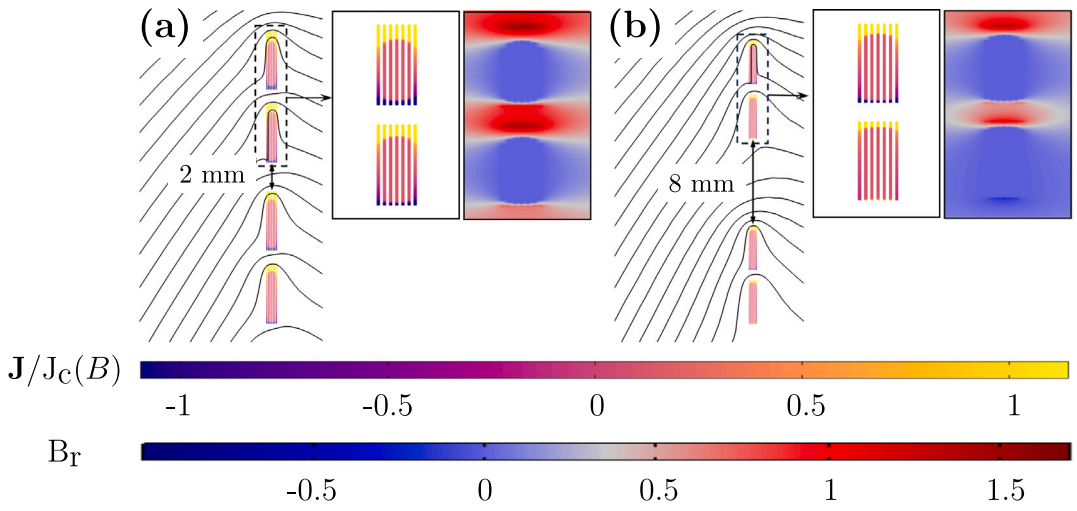

Fig. 7. Current distribution and magnetic field lines along with radial component of magnetic field in top cable: (a) with 2 mm axial gap between cables; (b) with 8 mm axial gap. All cases are under full-load condition and at t = 0.015 s. The aspect ratio of the zoomed cables was changed for better visibility.

The AC loss in the middle cables is primarily governed by the axial gap between the cables rather than by the winding height.

To investigate the impact of axial gap between the cables on the AC loss, the winding parameters are kept consistent with those listed for the LV winding in Table 3, except for the winding height, which varies according to the selected axial gap. In Fig. 6(a), as the axial gap increases from 2 mm to 16 mm, the winding height also increases; however, unlike in Fig. 4, the AC loss decreases. This behavior can be understood by comparing the changes in the end-cable losses shown in Fig. 5(b) and Fig. 6(b), where both cases involve similar differences in winding height. In Fig. 5(b), when the height increases due to the addition of turns, the end-cable loss increases only slightly. In contrast, in Fig. 6(b), as the height increases as the results of larger axial gap, the end-cable loss decreases significantly. This indicates that the influence of axial gap on AC loss is significantly more dominant than that of the winding height. Furthermore, as the axial gap increases, the end-cable loss decreases and the overall AC loss distribution becomes more uniform. In contrast, the AC loss in the middle of the winding is highest for the 16 mm gap and lowest for the 2 mm gap.

Fig. 7 shows the magnetic field distribution in the top cables for the axial gaps of 2 mm and 8 mm between cables. As the axial gap increases, the magnetic field lines become more parallel to the surface of the HTS tapes. The maximum magnitude of the radial field component decreases from 1.71 T at a 2 mm gap to 1.51 T at an 8 mm gap, which reduces the current penetration within the cable strands and, therefore, lowers the overall AC loss.

In summary, for a single LV winding (without the presence of an HV winding) and with a constant axial gap between the cables, the AC loss increases with increasing winding height. The increase in AC loss with winding height is stronger for a small axial gap (2 mm) than for a large axial gap (8 mm). In all cases, the majority of the AC loss occurs in the end cables.

By increasing the axial gap, the AC loss reduces gradually and exhibits a saturation-like behavior at larger gaps (starting at approximately 8 mm). This reduction is mainly caused by a significant decrease in the AC loss of the end cables. These results indicate that the influence of the axial gap on AC loss is more dominant than the influence of the winding height.

4.2. Combined low-voltage and high-voltage windings

In the combined LV and HV configuration, the distribution of the AC loss between the cables follows similar patterns as the single LV configuration. However, adding the HV winding with opposite current direction partially cancels the perpendicular field on the LV winding ends and reduces the AC loss. Furthermore, the magnetic field lines become more parallel between the LV and HV windings, which further reduces the AC loss in the LV winding.

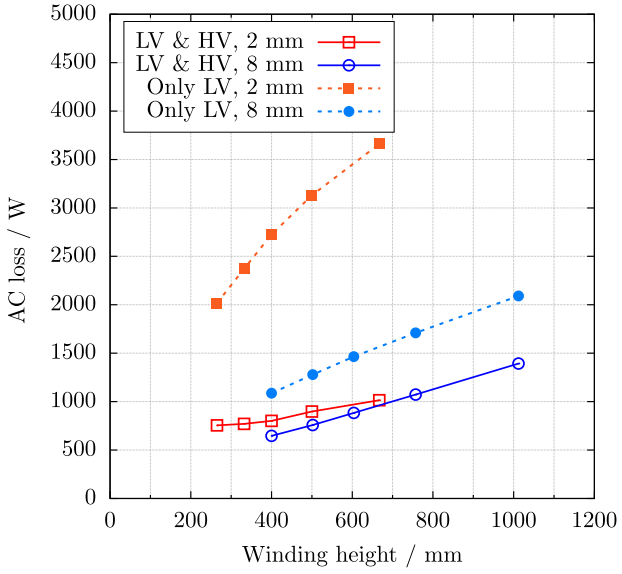

Fig. 8. Effect of height on the AC loss of LV winding, comparing the single LV winding configuration with the combined LV and HV winding configuration, considering 2 mm and 8 mm axial gap between cables. The height were increased by increasing the number of turns. All cases were calculated under full-load condition.

In Fig. 8, similar to Fig. 4, we investigated the impact of winding height on the AC loss of LV winding, this time including both HV and LV windings. The AC loss increases with height; However, compared to the single LV winding configuration, the rate of increase is smaller. This is expected, as the inclusion of both LV and HV windings reduces the end cable loss and consequently the rate of AC loss growth. The reduction in AC loss rate is more significant in the 2 mm gap case than in the 8 mm case, as the end cables loss in the single LV winding configuration was considerably higher with the 2 mm axial gap.

Fig. 9(a) compares the AC loss of the LV winding in the single LV configuration with that in the combined LV and HV configuration. As the axial gap increases, the AC loss of LV winding initially decreases

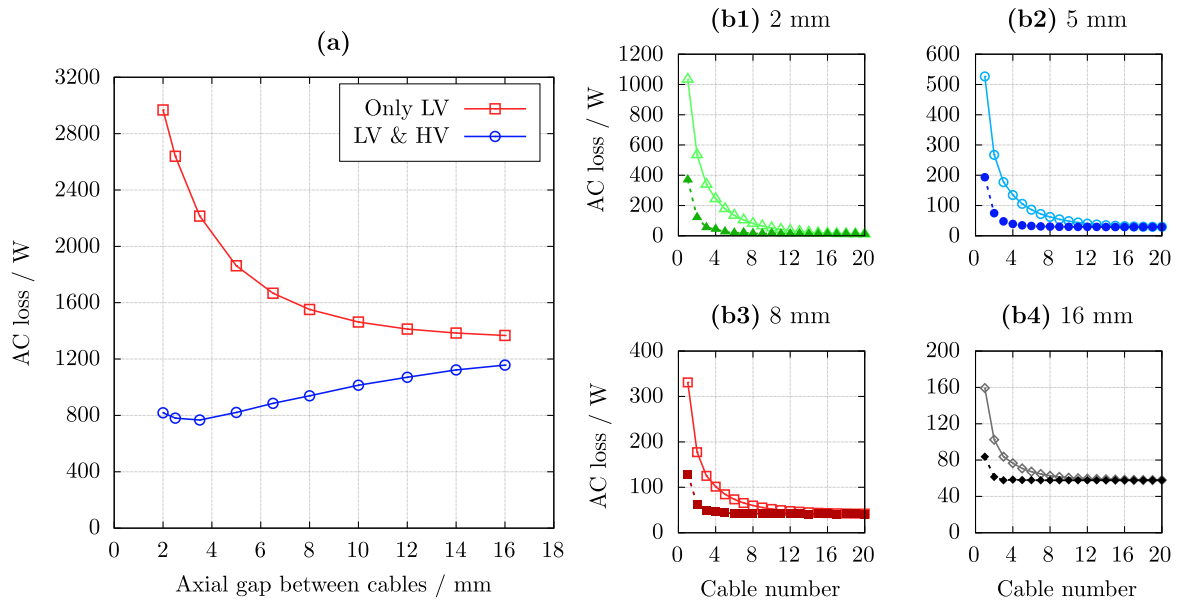

Fig. 9. (a) AC loss in the LV winding as a function of axial gap between cables, comparing the single LV winding configuration with the combined LV and HV winding configuration. (b1)–(b4) Distribution of AC loss among cables in the single LV winding (light colors, solid lines, unfilled markers) versus the combined LV and HV winding configuration (dark colors, dashed lines, filled markers) for different axial gaps: (b1) 2 mm, (b2) 5 mm, (b3) 8 mm, and (b4) 16 mm. All cases were calculated under full-load condition.

slightly up to a gap of 3.5 mm, and then increases with further gap enlargement, reaching a saturation at larger air gaps of approximately 16 mm. This trend contrasts with the continuous decrease observed in the single LV winding configuration. The underlying reason can be understood from Figs. 9(b1)–(b4). For example, at a 2 mm gap, the end-cable experiences an AC loss of around 1030 W in the single LV configuration, whereas adding the HV winding reduces this loss to around 370 W. This substantial loss reduction at the end-cable significantly lowers the total AC loss in the combined LV and HV configuration compared to the single case. As the axial gap increases, the difference in losses between the end and middle cables reduces, which explains why the AC losses of the two configurations converge at larger gaps, as shown in Fig. 9(a).

In general, in the combined LV and HV configuration, in comparison with the configuration with single LV winding, the observed differences arise from the partial cancellation of the strong perpendicular field at the end cables of the LV winding due to the presence of the HV winding. Similar to the single LV winding configuration, the AC loss increases with increasing height of both the HV and LV windings, but with a lower rate of increase. By increasing the axial gap, unlike the single LV winding configuration, the AC loss of the LV winding initially decreases slightly, then gradually increases and reaches a saturation at larger axial gaps.

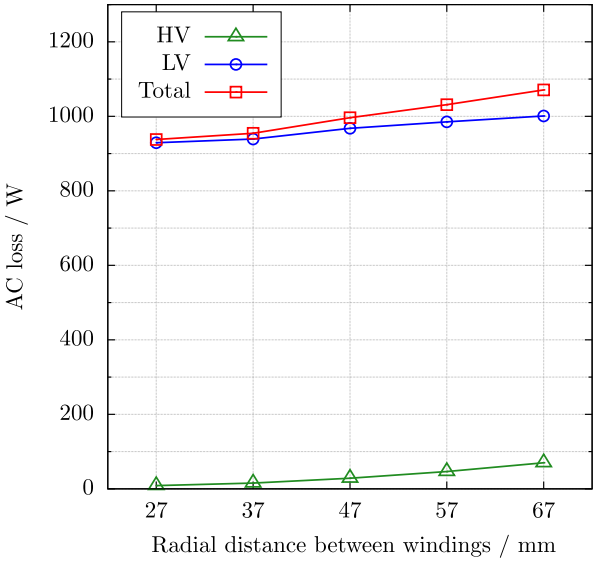

Fig. 10. Variation of HV, LV and total AC loss under full-load condition by altering the radial distance between LV and HV windings.

5. Influence of magnetic field cancellation

In the previous section, it was shown that adding the HV winding with an opposite current direction in a transformer reduces the AC loss by partially canceling the perpendicular component of the magnetic field at the end of the LV winding. Following the same principle, the AC loss can also be affected by changes in the radial distance between the LV and HV windings or by variations in the height of LV or HV windings, leading to unequal winding heights.

5.1. Influence of radial distance between LV and HV windings

Fig. 10 shows that increasing the radial distance between the LV and HV windings results in higher AC losses in both windings. This is due to reduced cancellation of the perpendicular component of magnetic field at the winding ends as the radial separation increases.

However, the radial spacing between the HV and LV windings directly influences the transformer's short-circuit impedance, which is a key design parameter. Therefore, the radial distance cannot be reduced below a certain limit without compromising the required short-circuit impedance.

5.2. Influence of height difference between LV and HV windings

To focus on the effect of height difference between the windings on AC loss and eliminate the other influencing factors such as variations in the axial gap between tapes, we kept the axial gap constant and

Table 4
Distribution of axial and radial turns for the LV and HV windings in the five design cases.

Parameter	Case 1	Case 2	Case 3	Case 4	Case 5
Axial HV turns per full layer/–	110	122	132	146	166
Axial HV turns in last layer/–	51	77	7	55	101
Radial layers (full + partial)/–	8 + 1	7 + 1	7 + 1	6 + 1	5 + 1
LV height/mm	661	661	661	661	661
HV height/mm	658	730	790	874	994
Height difference/%	0.4	10.4	19.5	32.2	50.3

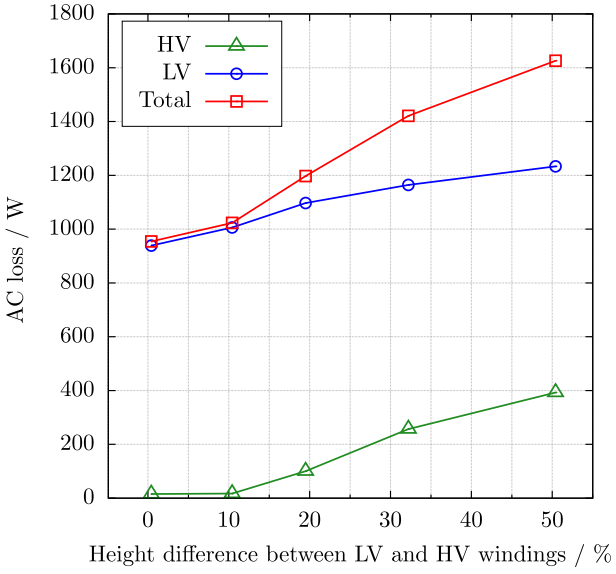

Fig. 11. Variation of HV, LV, and total AC losses under full-load condition as a function of the height difference between LV and HV windings (LV winding height kept constant).

varied only the height of the HV winding. This was achieved by increasing or decreasing the number of the layers in the radial direction, thereby decreasing or increasing the HV winding height, respectively. We considered five cases as tabulated in Table 4.

Fig. 11 shows the variation of HV, LV and total AC loss as a function of the height difference between the LV and HV windings under full-load conditions. The AC losses of LV and HV windings show an increasing trend with increasing height difference between the windings. This is due to a reduced cancellation of the perpendicular magnetic field component at the winding ends when the heights of the LV winding and the HV winding differ. These results indicate that for an optimized transformer design, the heights of the LV and HV windings should be as similar as possible.

Overall, increasing the radial spacing between the HV and LV windings leads to a slight increase in AC loss in both windings. Similarly, increasing the height difference between the HV and LV windings from 10% to higher values results in higher AC loss in both HV and LV windings. These behaviors occur because the cancellation of the perpendicular component of magnetic field at the winding ends is reduced.

6. Influence of parallel conductors

To investigate the impact of conductor parallelization on the AC loss of the LV winding, simulations were carried out with varying numbers of strands while keeping the total current constant. The model included both HV and LV windings; however the focus here is on the LV winding, as the AC loss in the HV winding stays nearly unchanged across all cases. Fig. 12 illustrates the dependence of the AC loss in watts, the

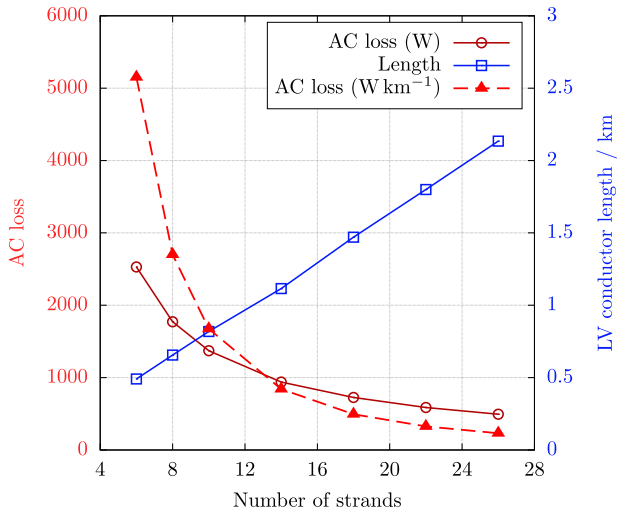

Fig. 12. Variation of AC loss of LV winding in watts (dark red, unfilled circles), AC loss divided by the total conductor length (light red, filled triangles), and LV conductor length (blue, unfilled squares) as functions of the number of parallel strands in the winding. All cases were calculated under full-load condition.

total LV winding length, and the AC loss divided by the LV winding length (W km^{-1}) on the number of strands.

As the number of parallel strands increases, the AC loss decreases continuously. This trend occurs because the current per strand decreases, leading to a smaller current penetration within each strand and associated AC loss. However, increasing the number of parallel conductors also increases the total conductor length, leading to a higher material cost. To identify a practical compromise, the AC loss per kilometer is analyzed. The AC loss per km decreases sharply up to around 18 strands, after which the reduction rate becomes more gradual but still continues. Therefore, considering both the AC loss reduction and the increase in conductor length, employing at least around 18 strands per cable provides an effective balance between efficiency and conductor usage.

7. Influence of voltage per turn

The voltage per turn, u_w, is a key design parameter in transformers, as it directly influences the core radius and size (and thus the overall weight), as well as the number of turns (and thus the winding height). These two factors together influence the total conductor length and hence the HTS transformer cost. However, the impact of u_w on the AC loss is more complex, as its variation simultaneously changes multiple geometric aspects of the transformer winding.

The u_w is proportional to the square of the core radius (Kalsi, 2011). Therefore, as the u_w increases, the radii of both the LV and HV windings increase accordingly. In addition, the number of LV and HV turns is determined by dividing the maximum voltage by u_w; hence, a higher u_w results in fewer turns and lower height.

To investigate the influence of u_w on AC loss, we analyzed eight design cases, combining four u_w values of 30 V, 40 V, 50 V and 60 V, with two axial gap configurations of 2 mm and 8 mm. Table 5 summarizes the main design parameters of the HV and LV windings at different u_w values, including geometric parameters, conductor length, and core weight. Parameters not listed in this table are identical to those given for the 45 V-per-turn case in Table 3.

Table 6 shows the calculated AC loss at the full load. Fig. 13 presents the total AC loss and total conductor length as a function of u_w for two configurations, with 2 mm and 8 mm axial gap between cables. For the 8 mm gap configuration, the total AC loss follows the trend of the

Table 5
Main design parameters of the transformer for different voltage per turn values..

Voltage per turn	30 V		40 V		50 V		60 V	
Parameter	LV	HV	LV	HV	LV	HV	LV	HV
2 mm gap design								
Radius/mm	290.0	340.0	320.7	370.8	348.5	394.2	372.5	422.6
Height/mm	667.5	670.0	500.0	502.0	399.5	406.0	332.5	334.0
Axial turns per full layer/–	20	112	15	84	12	66	10	56
Axial turns in last layer/–	N/A[a]	52	N/A[a]	40	N/A[a]	46	N/A[a]	26
Radial layers (full + partial)/–	1	12+1	1	12+1	1	12+1	1	12+1
Total turns/–	20	1396	15	1047	12	838	10	698
Conductor length/km phase^{-1}	1.530	2.982	1.270	2.440	1.102	2.095	0.983	1.850
Core weight/t	6.072		7.923		9.950		12.07	
8 mm gap design								
Radius/mm	290.0	335.7	320.5	365.2	348.5	394.2	372.5	417.0
Height/mm	1012	1006	757	754	604	598	502	502
Axial turns per full layer/–	20	126	15	126	12	100	10	84
Axial turns in last layer/–	N/A[a]	40	N/A[a]	39	N/A[a]	38	N/A[a]	26
Radial layers (full + partial)/–	1	8+1	1	1 + 8	1	8+1	1	8+1
Total turns/–	20	1396	15	1047	12	838	10	698
Conductor length/km phase^{-1}	1.530	2.945	1.270	2.411	1.102	2.074	0.983	1.835
Core weight/t	6.925		8.756		10.72		12.86	

[a] LV has no partial last layer; last layer equals a full layer.

Table 6
Calculated AC losses of different designs for various u_w and axial gaps from Table 5.

AC Loss/W	30 V		40 V		50 V		60 V	
	LV	HV	LV	HV	LV	HV	LV	HV
2 mm gap	843.5	39.2	849.6	40.3	891.3	39.1	876.4	47.2
8 mm gap	1200	16.1	1025	14.8	921.5	15.0	850.6	13.0

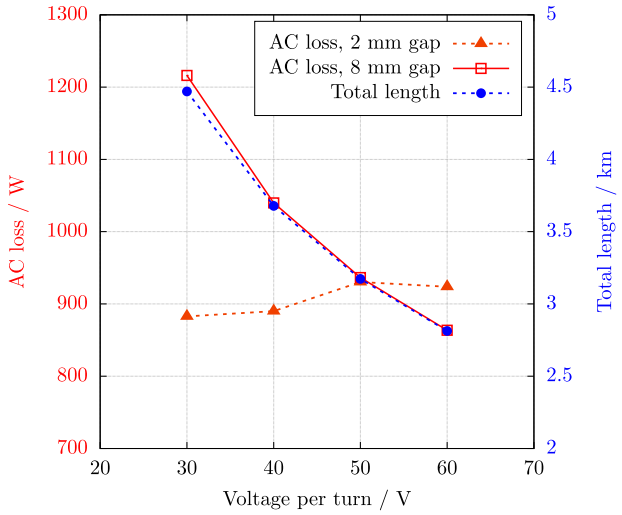

Fig. 13. AC loss and total length in terms of Voltage per turn for two configurations with 2 mm and 8 mm axial gap between cables under full-load condition adopted for 20 K.

total conductor length. In contrast, for the 2 mm gap configuration, the total AC loss remains relatively stable, ranging between 843 W and 891 W. As shown in Figs. 9(b1) and 9(b3), the AC loss for 2 mm gap configuration is concentrated at the winding ends. This explains why the total AC loss remains relatively unaffected by variation in the number of turns and conductor length. Conversely, in 8 mm gap configuration, the AC loss is more uniformly distributed throughout the winding, resulting in a stronger correlation with the number of turns and total conductor length.

Therefore, the influence of voltage per turn on AC loss strongly depends on the axial gap. At a small axial gap (2 mm), the AC loss increases only slightly with increasing u_w, whereas at a large gap (8 mm gap), the AC loss decreases with increasing u_w and is closely related to the conductor length.

Table 7
Optimized parameters of the MFDs of LV winding used in the transformer design operating at 20 K.

Parameters	LV
Radius/mm	320
Width/mm	30
Height/mm	15
Distance to end/mm	2

8. Influence of iron core and magnetic flux divertor

Any transformer component that diverts the magnetic field can influence the AC loss in the windings, either positively or negatively. This includes components made of ferromagnetic materials, such as the iron core and the magnetic flux diverters (MFDs).

8.1. Iron core

In the iron core, the degree of magnetic field diversion and its effect on AC loss is determined by two factors: the radial distance between the core and the windings, and the relative permeability (μ_r) of the core material.

In this study, we selected silicon steel NGO 50PN270 for the transformer core. At full load, the presence of the iron core results in approximately only 2.5% increase in total AC loss. This relatively small impact can be attributed to the strong magnetic field between the LV and HV windings, which shields the winding and reduce the impact of the iron core (Wu et al., 2024).

8.2. Magnetic flux divertor

MFDs are circular rings made of ferromagnetic material placed at top and bottom of the HV and/or LV windings. They divert the radial component of the magnetic field, aligning it more parallel to the tape surface at the winding ends and thereby diminishing the AC loss within the windings. However, a drawback of MFDs is the potential for high

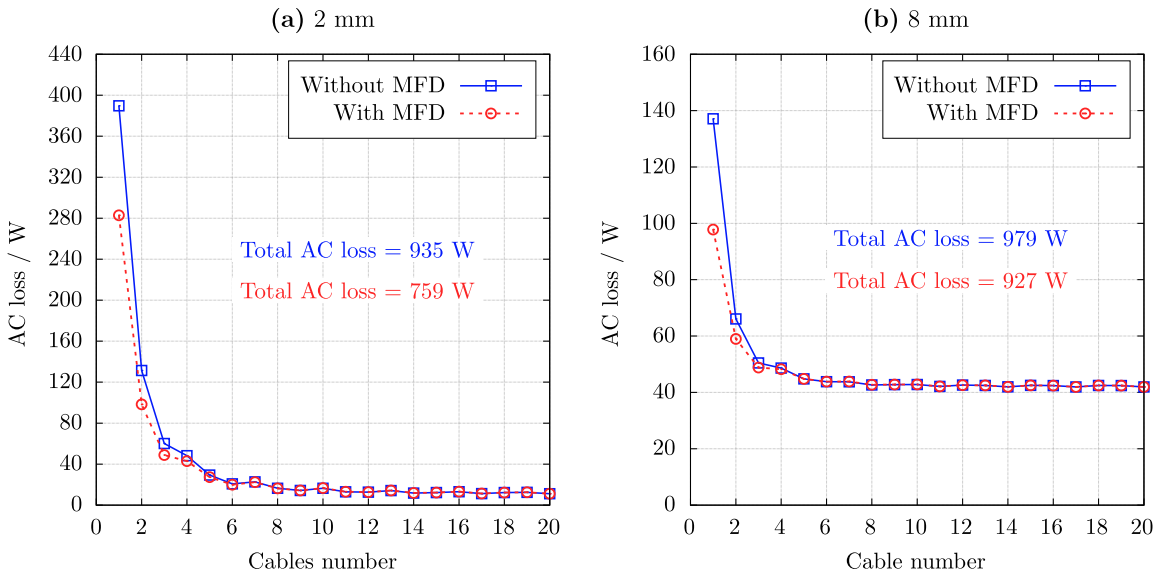

Fig. 14. Distribution of AC loss in the LV winding among cables, with and without the inclusion of optimized MFDs, for different axial gaps between cables: (a) 2 mm, (b) 8 mm. All cases were calculated under full-load conditions.

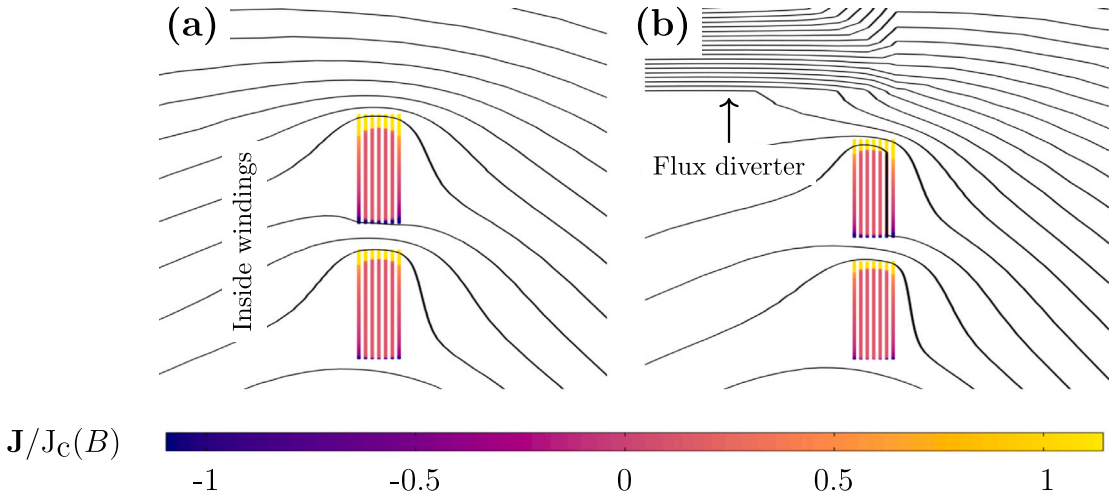

Fig. 15. Current distribution and magnetic field lines in top cable: (a) without magnetic flux diverter; (b) with magnetic flux diverter. All cases are under full-load condition and at t = 0.015 s. The aspect ratio of the cables was changed for better visibility.

additional AC losses and heat production. To mitigate this issue, one or several gaps containing insulating material can be incorporated into the ring. Additionally, MFDs can be constructed using a low-loss material such as silicon steel sheets with insulating materials (Zhao et al., 2023; Staines et al., 2012). By utilizing this low-loss material, the AC loss of the MFD can be diminished to an almost negligible level (Zhao et al., 2023).

In the designed transformer operating at 20 K, a MFD ring with rectangular cross-section was included for LV winding only, made of silicon steel NGO 50PN270 material. No MFD was applied to the HV winding due to its relatively low AC loss. We optimized several parameters such as height (axial direction), width (radial direction), axial distance from the windings end, and the position, through extensive trial and error. The final optimized values are listed in Table 7.

The optimized MFD was implemented in LV winding for two configurations (see Table 3) with axial gaps of 2 mm and 8 mm. For the LV winding with a 2 mm axial gap, the total AC loss was reduced by 19%. In contrast, for the 8 mm gap configuration, the reduction in AC loss was about 5%. Figs. 14(a) and (b) show that the MFD mainly influences the first and second end-cables. In 2 mm winding configuration, most of the AC loss is concentrated in a few end-cables, making the MFD highly effective. In contrast, in 8 mm gap configuration, the AC loss is more evenly distributed across the winding, which reduces the effectiveness of the MFD. Fig. 15 shows the current distribution and magnetic field lines in the top cables with and without including MFD. The MFD diverts the magnetic field lines around the first cable and make it more parallel to the tape surface.

Table 8
Main design parameters of the HV and LV windings and parameters of MFDs for voltage per meter of 45 V at 20 K, 70 K and 77 K.

Temperature	20 K		70 K		77 K-15P		77 K-18P	
Parameter	LV	HV	LV	HV	LV	HV	LV	HV
Winding configuration								
Radius/mm	334.7	381.6	306.5	357.6	306.5	370	306.5	366.6
Height/mm	570	574	570	574	713	706	856	850
Parallel conductor (Axial, Radial)	4, 1	1, 1	4, 3	2, 1	5, 3	3, 1	6, 3	3, 1
Axial turns per full layer/–	42	96	52	96	65	118	78	142
Axial turns in last layer/–	N/A[a]	67	N/A[a]	38	N/A[a]	79	N/A[a]	95
Radial layers (full + partial)/–	1	9+1	3	19+1	3	23+1	3	19+1
Total turns/–	13	931	13	931	13	931	13	931
Axial gap (non-par, par)/mm	2, 2	2, 2	2, 2	2, 2	2, 2	2, 2	2, 2	2, 2
Radial gap/mm	N/A	2	1	2	1	2	2	1
Conductor length/km phase^{-1}	1.53	2.23	4.2	4.19	5.26	6.49	6.31	6.43
Core weight/t	9.362		8.913		9.62		10.11	
Magnetic flux diverter								
Radius/mm	314.5	399.5	328.5	373	288.5	380.5	288.5	374
Width/mm	40	55	40	55	40	70	40	55
Height/mm	15	15	15	15	15	15	15	15
Distance to end/mm	2	5	2	5	2	5	2	5

[a] LV has no partial last layer; last layer equals a full layer.

9. Influence of operating temperature

Based on the AC loss mitigation strategies proposed in the previous sections, we developed four transformer designs for operating temperatures of 20 K, 70 K and 77 K. In these designs, we sought a compromise among the three key objectives of low weight, high efficiency and reduced cost. The transformer models includes all the electromagnetic components such as the core and the optimized flux diverters.

As shown in Fig. 2, the self-field critical current of the 4 mm Fujikura tape is 2405 A at 20 K, decreasing to 483 A and 303 A at 70 K and 77 K, respectively. The reduction in critical current with increasing temperature necessitates the use of additional parallel cables and tapes, which increases the total conductor length and the overall costs of the transformer.

Table 8 lists the main design parameters of the HV and LV windings, as well as the MFDs configuration, for the 45 V voltage per meter designs at 20 K, 70 K, and two different designs at 77 K: one using 15 parallel cables per turn (77 K-15P) and another using 18 parallel cables per turn (77 K-18P). Table 9 shows the calculated AC loss of the LV and HV windings, along with the total AC loss at various load levels for all the proposed designs.

Fig. 16(a) compares the total AC loss per phase at three different operating temperature designs. At 20 K, the self-field critical current of the tape is approximately 5 and 8 times higher than at 70 K and 77 K, respectively. By increasing the total tape length, we were able to prevent the AC loss at 70 K and 77 K from increasing proportionally to the critical current. The AC losses under full-load condition for the operating temperatures of 20 K, 70 K and 77 K-18P are 298 W, 640 W and 342 W, respectively. This means that the AC loss at 70 K and 77 K-18P was increased 110% and 15%, compared to the AC loss at 20 K, respectively.

Comparing the two designs at 77 K, the 77 K-18P configuration requires approximately 1 km more HTS tapes (an 8% increase), and results in a 0.49 t higher core weight (a 5% increase). However, 77 K-18P design reduces the total AC loss at full load by 204 W (a 37% decrease). Although the additional conductor length slightly increased the material cost, the substantial reduction in AC loss reduces the thermal load on the cryogenic system and can therefore reduces the operating cost. These results highlights the trade-off between weight, cost and AC loss in the HTS transformer design, emphasizing that there should be a compromise between them.

Up to this point, the term AC loss has referred to the heat generated at cryogenic temperature. In an HTS transformer, however, the cryogenic system must remove this heat to the ambient environment. Due to the limited efficiency of cryocoolers, extracting 1 W of heat at cryogenic temperature requires considerably higher electrical power at room temperature. This ratio, known as the cooling factor, depends primarily on the operating temperature and the efficiency of the cryogenic system (Ter Brake and Wiegerinck, 2002). Based on the information obtained from the manufactures, the cooling factors are approximately 79, 26 and 21 for various cryocoolers operating at 20 K (Vorbuchner, 2024), 70 K (Absolute Systems Ltd., 2024) and 77 K (Sumitomo Heavy Industries, 2025), respectively. Fig. 16(b) compares the total AC loss per phase at room temperature for different operating temperatures. We observe that, although at cryogenic temperature the transformer designed for 20 K exhibits the lowest AC loss, at room temperature the design operating at 77 K becomes the most efficient.

Table 9
Calculated LV, HV and total AC loss per phase for various loads for the developed transformer designs at 20 K, 70 K and 77 K.

$I_t I_n^{-1}$	LV/W	HV/W	Total/W
20 K			
0.25	3.05	0	3.05
0.5	31.9	0.5	32.4
0.75	113.1	3.7	116.8
1	288.3	9.5	297.8
70 K			
0.25	10.3	1.8	12.1
0.5	76	13	89
0.75	236	39	275
1	550	90	640
77 K-15P			
0.25	10.8	1.5	12.3
0.5	72	10	82
0.75	216.4	28.2	244.6
1	481.8	65.1	546.9
77 K-18P			
0.25	6.3	1.1	7.4
0.5	43.8	6.7	50.5
0.75	135.8	20.8	156.6
1	297.5	45	342.5

10. Conclusion

We conducted a comprehensive investigation on practical strategies for mitigating AC loss in a 15 MVA HTS transformer. Using the efficient T-A formulation model, we calculated the AC loss in up to 6000 tapes in the LV and HV windings in detail. We evaluated the influence of

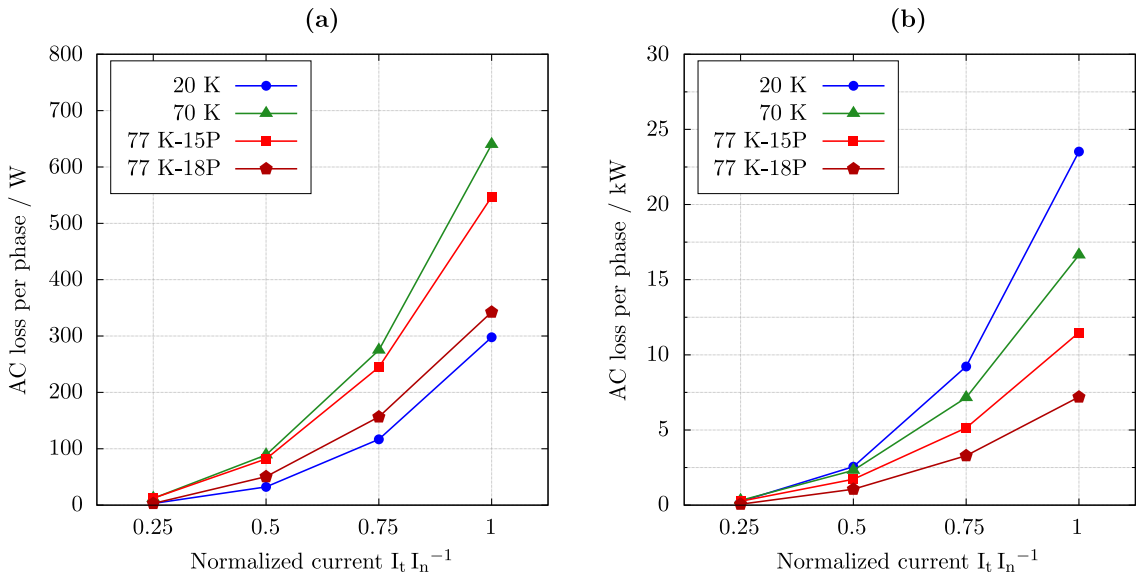

Fig. 16. Comparison of total AC loss per phase at three operating temperatures of 20 K, 70 K and 77 K: (a) at cryogenic temperatures and (b) at room temperature.

key design and operating parameters on the AC loss, including winding height, axial gap between the cables, radial distance between HV and LV winding, winding height difference, number of parallel conductors, voltage per turn, magnetic flux diverters, and temperature. Based on the insights obtained, we proposed four improved transformer designs at operating temperatures of 20 K, 70 K, and two configurations at 77 K that balance AC loss reduction with conductor cost and core weight. We have compared their AC loss, conductor length and core weight. Some of the key conclusions, design principles and practical strategies for AC loss mitigation are as follows:

- Increasing the height of both the LV and HV windings while keeping the axial gap constant leads to an increase in AC loss.
- The AC loss increases gradually with increasing the axial gap between cables in LV winding and tends to approach a saturation-like behavior at larger gaps.
- Reducing the radial distance between the LV and HV windings leads to a moderate reduction in AC loss.
- Increasing the height difference between the HV and LV windings results in an increase in AC loss.
- When using Roebel cable as LV winding, employing at least around 18 strands per cable provides an effective balance between efficiency and conductor usage.
- The influence of voltage per turn on AC loss strongly depends on the axial gap between the LV winding cables. At a small axial gap (e.g. 2 mm), the AC loss increases only slightly with increasing u_w, whereas at a large axial gap (e.g. 8 mm gap), the AC loss decreases as u_w increases and is closely related to the conductor length.
- Including MFDs with an optimum size and position with respect to the winding end in the transformer design effectively reduces the AC loss. However, this reduction is more pronounced for a small axial gap between the LV winding cables (e.g. 2 mm) than for a large gap (e.g. 8 mm).
- At higher operating temperature, the lower critical current of the HTS tapes requires the use of more parallel HTS conductor, which increases the overall cost of the transformer. Therefore, a compromise must be made between the amount of conductor used and the resulting AC loss of the transformer.

This research offers valuable insights and approaches for designing, optimizing, and developing HTS transformers to be more energy-efficient, compact, lightweight and cost-effective.

CRediT authorship contribution statement

Asef Ghabeli: Writing – original draft, Writing – review & editing, Visualization, Software, Validation, Methodology, Investigation, Formal analysis, Data curation, Conceptualization. **Mathias Noe:** Writing – review & editing, Validation, Supervision, Resources, Project administration, Investigation, Funding acquisition, Methodology, Conceptualization. **Stephan Rother:** Resources, Validation, Writing – Review & Editing. **Christian Schacherer:** Resources, Validation, Writing – Review & Editing. **Aime Mbuy:** Resources, Validation, Writing – Review & Editing. **Jürgen Gangel:** Resources, Validation, Writing– Review & Editing. **Francesco Grilli:** Writing – review & editing, Validation, Supervision, Methodology, Investigation, Formal analysis, Conceptualization.

Declaration of competing interest

The authors declare the following financial interests/personal relationships which may be considered as potential competing interests: Asef Ghabeli reports financial support was provided by Siemens Energy. Asef Ghabeli reports a relationship with Siemens Energy that includes: funding grants. If there are other authors, they declare that they have no known competing financial interests or personal relationships that could have appeared to influence the work reported in this paper.

Acknowledgments

The authors acknowledge financial support from Siemens Energy.

Appendix A

As shown in Fig. 17, the original measured $I_c(B,\theta)$ data of Fujikura FYSC tape at 20 K exhibit no symmetry with respect to 90°, which is a common characteristic of many commercial superconducting tapes. The angle corresponding to the maximum critical current shifts from approximately 78° at 0.1 T to 86° at 1.5 T. To achieve a smoother fitting behavior and to make the dataset more representative of typical commercial superconducting tapes, we symmetrized the measured data artificially. As described in Section 2.2, we used Eq. (2) to fit the symmetrized measurement data (see Fig. 18). To ensure that symmetrization did not significantly affect the calculated AC loss, we

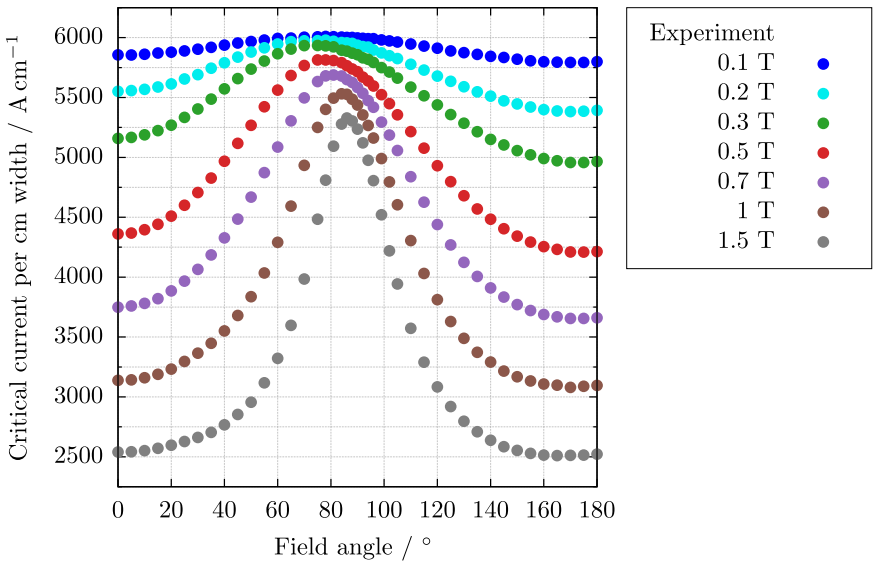

Fig. 17. Original measured $I_c(B,\theta)$ data of Fujikura FYSC tape at 20 K under various magnetic fields and orientations. The field angle is defined with respect to the normal vector of the tape surface. The data were obtained from the Wimbush database, created by Robinson Research Institute in New Zealand (Strickland et al., 2014).

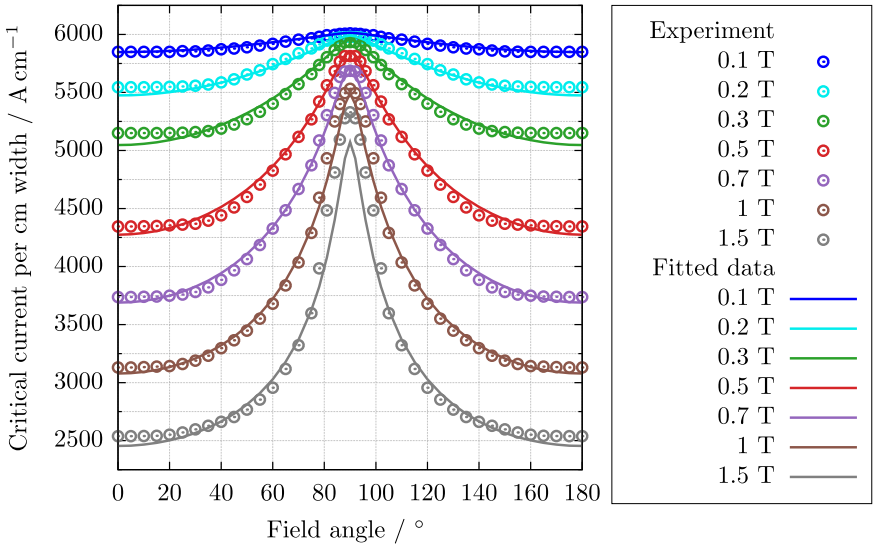

Fig. 18. Symmetrized measured $I_c(B,\theta)$ data of Fujikura FYSC tape with respect to 90 degree and the fitted data using Eq. (2) at 20 K under various magnetic fields and orientations. The field angle is defined with respect to the normal vector of the tape surface.

modeled the LV winding (see Table 3) using both the original and the symmetrized $I_c(B,\theta)$ data. The resulting AC losses differed by only about 3%, confirming that the symmetrization process had a negligible impact on the loss estimation.

Data availability

Data will be made available on request.

References

Absolute Systems Ltd., 2024. Turbo-Brayton cryocooler (70 k class): Technical datasheet [online].

Berger, A., 2011. Entwicklung Supraleitender, Strombegrenzender Transformatoren. KIT Scientific Publishing, Karlsruhe.

Berger, A., Noe, M., Kudymow, A., 2011. Test results of 60 kVA current limiting transformer with full recovery under load. IEEE Trans. Appl. Supercond. 21 (3), 1384–1387.

Dai, S., Ma, T., Qiu, Q., Zhu, Z., Teng, Y., Hu, L., 2016. Development of a 1250-kVA superconducting transformer and its demonstration at the superconducting substation. IEEE Trans. Appl. Supercond. 26 (1).

Fang, X., Wang, X., Sun, Y., Song, W., Pei, X., Jiang, Z., Badcock, R., Long, N., Fang, J., 2021. Application of Flux Diverters in High Temperature Superconducting Transformer Windings for AC Loss Reduction. IEEE Trans. Appl. Supercond. 31 (8), 1–5.

Ghabeli, A., Besmi, M.R., 2017. Capability of new multi-segment winding configurations in HTS transformer to mitigate electromagnetic forces under short-circuit condition. Cryogenics 84, 20–28.

Ghabeli, A., Yazdani-Asrami, M., Besmi, M.R., Gholamian, S.A., 2015a. Optimization of Distributive Ratios of Apportioned Winding Configuration in HTS Power Transformers for Hysteresis Loss and Leakage Flux Reduction. J. Supercond. Nov. Magn. 28 (12), 3463–3479.

Ghabeli, A., Yazdani-Asrami, M., Gholamian, S.A., 2015b. A Novel Unsymmetrical Multi-Segment Concentric Winding Scheme for Electromagnetic Force and Leakage Flux Mitigation in HTS Power Transformers. IEEE Trans. Appl. Supercond. 25 (6), 1–10.

Glasson, N., Staines, M., Jiang, Z., Allpress, N., 2013. Verification testing for a 1 MVA 3-phase demonstration transformer using 2G-HTS roebel cable. IEEE Trans. Appl. Supercond. 23 (3).

Glasson, N., et al., 2017. Test results and conclusions from a 1 MVA superconducting transformer featuring 2G HTS roebel cable. IEEE Trans. Appl. Supercond. 27 (4), 1–5.

Gömöry, F., Šouc, J., Adámek, M., Ghabeli, A., Solovyov, M., Vojenčiak, M., 2019. Impact of critical current fluctuations on the performance of a coated conductor tape. Supercond. Sci. Technol. 32 (12), 124001.

Hellmann, S., Abplanalp, M., Elschner, S., Kudymow, A., Noe, M., 2019. Current limitation experiments on a 1 MVA-class superconducting current limiting transformer. IEEE Trans. Appl. Supercond. 29 (5).

Hellmann, S., Abplanalp, M., Hofstetter, L., Noe, M., 2017. Manufacturing of a 1-MVA-class superconducting fault current limiting transformer with recovery-under-load capabilities. IEEE Trans. Appl. Supercond. 27 (4).

Huber, F., Song, W., Zhang, M., Grilli, F., 2022. The T-A formulation: an efficient approach to model the macroscopic electromagnetic behaviour of HTS coated conductor applications. Supercond. Sci. Technol. 35 (4), 043003.

Jiang, Z., Song, W., Pei, X., Fang, J., Badcock, R.A., Wimbush, S.C., 2021. 15% reduction in AC loss of a 3-phase 1 MVA HTS transformer by exploiting asymmetric conductor critical current. J. Phys. Commun. 5 (2), 025003.

Jose, G., Chacko, R., 2014. A review on wind turbine transformers. In: 2014 Annual International Conference on Emerging Research Areas: Magnetics, Machines and Drives (AICERA/ICMMD). IEEE, Kottayam, India, India, pp. 1–7.

K., Jong-Tae, K., Woo-Seok, K., Sung-Hoon, C., Kyeong-Dal, H., Jin-Ho, H., Gye-Won, H., Song-Yop, 2005a. Analysis of AC losses in HTS pancake windings for transformer according to the operating temperature. IEEE Trans. Magn. 41 (5), 1888–1891.

Kajikawa, K., Funaki, K., 2012. Reduction of Magnetization in Windings Composed of HTS Tapes. IEEE Trans. Appl. Supercond. 22 (3), 4400404.

Kalsi, S.S., 2011. Applications of High Temperature Superconductors to Electric Power Equipment. John Wiley & Sons.

Kim, Y.B., Hempstead, C.F., Strnad, A.R., 1962. Critical Persistent Currents in Hard Superconductors. Phys. Rev. Lett. 9 (7), 306–309.

Kim, J.-T., Kim, W.-S., Kim, S.-H., Choi, K.-D., Hong, G.-W., Joo, H.-G., Hahn, S., 2005b. Optimization of Transformer Winding Considering AC Loss of BSCCO Wire. IEEE Trans. Appiled Supercond. 15 (2), 1839–1842.

Li, X., Ren, L., Xu, Y., Shi, J., Chen, X., Chen, G., Tang, Y., Li, J., 2021. Calculation of CORC cable loss using a coupled electromagnetic-thermal T-A formulation model. IEEE Trans. Appl. Supercond. 31 (4), 1–7.

Li, X., Wu, S., Zhou, Y., Hu, G., Long, G., 2008. Influence of high temperature superconducting transformer geometry on leakage magnetic field. IEEE Trans. Magn. 44 (4), 492–496.

Liang, F., Venuturumilli, S., Zhang, H., Zhang, M., Kvitkovic, J., Pamidi, S., Wang, Y., Yuan, W., 2017. A finite element model for simulating second generation high temperature superconducting coils/stacks with large number of turns. J. Appl. Phys. 122 (4), 043903.

Mellerud, R., Hartmann, C., Klop, C. Leonard, Nøland, J.K., 2024. Influence of eddy current losses in nonsuperconducting layers of HTS in superconducting electrical machines. IEEE Trans. Appl. Supercond. 34 (7), 1–7.

Pardo, E., Staines, M., Jiang, Z., Glasson, N., 2015. Ac loss modelling and measurement of superconducting transformers with coated-conductor Roebel-cable in low-voltage winding. Supercond. Sci. Technol. 28 (11), 114008.

Schlosser, R., Schmidt, H., Leghissa, M., Meinert, M., 2003. Development of high-temperature superconducting transformers for railway applications. IEEE Trans. Appl. Supercond. 13 (2), 2325–2330.

Solovyov, M., Pardo, E., Šouc, J., Gömöry, F., Skarba, M., Konopka, P., Pekarčíková, M., Janovec, J., 2013. Non-uniformity of coated conductor tapes. Supercond. Sci. Technol. 26 (11), 115013.

Song, W., Jiang, Z., Staines, M., Wimbush, S., Badcock, R., Fang, J., 2020. AC Loss Calculation on a 6.5 MVA/25 kV HTS Traction Transformer With Hybrid Winding Structure. IEEE Trans. Appl. Supercond. 30 (4), 1–5.

Song, W., Jiang, Z., Zhang, X., Staines, M., Badcock, R.A., Fang, J., Sogabe, Y., Amemiya, N., 2018. AC loss simulation in a HTS 3-Phase 1 MVA transformer using H formulation. Cryogenics 94, 14–21.

Staines, M., Glasson, N., Pannu, M., Thakur, K.P., Badcock, R., Allpress, N., D'Souza, P., Talantsev, E., 2012. The development of a Roebel cable based 1 MVA HTS transformer. Supercond. Sci. Technol. 25 (1), 014002.

Strickland, N.M., Hoffmann, C., Wimbush, S.C., 2014. A 1 kA-class cryogen-free critical current characterization system for superconducting coated conductors. Rev. Sci. Instrum. 85 (11), 113907.

Sumitomo Heavy Industries, 2025. SRP-160d2 cryocooler: Technical specifications. Manufacturer datasheet.

Ter Brake, H.J.M., Wiegerinck, G.F.M., 2002. Low-power cryocooler survey. Cryogenics 42 (11), 705–718.

U.S. Department of Energy, 2023. Wind turbines: Bigger, better. (Accessed 24 June 2024).

Vargas-Llanos, C.R., Huber, F., Riva, N., Zhang, M., Grilli, F., 2022. 3D homogenization of the T-A formulation for the analysis of coils with complex geometries. Supercond. Sci. Technol. 35 (12), 124001.

Vargas-Llanos, C.R., Krämer, J., Noe, M., Grilli, F., 2023. Design and test of a setup for calorimetric measurements of AC transport losses in HTS racetrack coils. Supercond. Sci. Technol. 36 (4), 045015.

Vargas-Llanos, C.R., Lengsfeld, S., Grilli, F., 2020. T-A Formulation for the Design and AC Loss Calculation of a Superconducting Generator for a 10 MW Wind Turbine. IEEE Access 8, 208767–208778.

Vargas-Llanos, C.R., Lengsfeld, S., Noe, M., Arndt, T., Grilli, F., 2021. Influence of Coil Position on AC Losses of Stator Superconducting Windings of a Synchronous Machine for a 10 MW Wind Turbine. IEEE Trans. Appl. Supercond. 31 (7), 1–9.

Vorbuchner, M., 2024. Turbo-brayton cryocooling for HTS applications. Presented at the ZIEHL Workshop, Berlin.

Wu, Y., Song, W., Wimbush, S.C., Fang, J., Badcock, R.A., Long, N.J., Jiang, Z., 2023. Combined Impact of Asymmetric Critical Current and Flux Diverters on AC Loss of a 6.5 MVA/25 kV HTS Traction Transformer. IEEE Trans. Transp. Electrific. 9 (1), 1590–1604.

Wu, Y., You, S., Fang, J., Badcock, R.A., Long, N.J., Jiang, Z., 2024. AC loss study on a 3-phase HTS 1 MVA transformer coupled with a three-limb iron core. Superconductivity 10, 100095, Publisher: Elsevier BV.

Zhang, H., Zhang, M., Yuan, W., 2017a. An efficient 3D finite element method model based on the *T-A* formulation for superconducting coated conductors. Supercond. Sci. Technol. 30 (2), 024005.

Zhang, X., Zhong, Z., Ruiz, H.S., Geng, J., Coombs, T.A., 2017b. General approach for the determination of the magneto-angular dependence of the critical current of YBCO coated conductors. Supercond. Sci. Technol. 30 (2), 025010.

Zhao, X., Fang, J., Jiang, Z., Song, W., Liu, N., Gao, Y., Li, X., Zeng, F., Xia, Y., Badcock, R.A., Long, N.J., Staines, M.P., Buckley, R.G., Fang, X., Li, Y., Liu, B., Zhang, J., Han, W., Li, L., Wang, J., Gao, P., 2023. Design, development, and testing of a 6.6 MVA HTS traction transformer for high-speed train applications. Supercond. Sci. Technol. 36 (8), 085009.

Zhou, P., Dos Santos, G., Ghabeli, A., Grilli, F., Ma, G., 2022. Coupling electromagnetic numerical models of HTS coils to electrical circuits: multi-scale and homogeneous methodologies using the T-A formulation. Supercond. Sci. Technol. 35 (11), 115005.

Zhou, P., Ghabeli, A., Ainslie, M., Grilli, F., 2023. Characterization of flux pump-charging of high-temperature superconducting coils using coupled numerical models. Supercond. Sci. Technol. 36 (11), 115002.

Zueger, H., 1998. 630 kVA high temperature superconducting transformer. Cryogenics 38 (11), 1169–1172.